Materials & Design 231 (2023) 112061

Contents lists available at ScienceDirect

Materials & Design

journal homepage: www.elsevier.com/locate/matdes

Flexible and conductive core-sheath fiber using multifunctional merocyanine as a smart electrolyte for a high-performance fibrous visible light sensor

Guiqing Dang [a], Longfei Fan [a,*], Kaifang Chen [a], Ronghua Hu [a], Yuncong Luo [a], Yutao Huang [a], Qinghua Wu [a], Min Zhu [b], John H. Xin [c], Hanlun Lu [d,*], Feng Gan [a,*]

[a] School of Textile Materials and Engineering, Wuyi University, Jiangmen, Guangdong 529020, China
[b] School of Chemistry, Sun Yat-Sen University, Guangzhou 510275, China
[c] Institute of Textiles & Clothing, The Hong Kong Polytechnic University, Hung Hom, Kowloon, Hong Kong, China
[d] Institute of Mass Spectrometry and Atmospheric Environment, Guangdong Provincial Engineering Research Center for On-line Source Apportionment System of Air Pollution, Jinan University, Guangzhou, China

HIGHLIGHTS

- A negative spiropyran with a visible light response is successfully synthesized.
- Merocyanine diol is first used as an intelligent electrolyte.
- A visible light sensor with a simple structure is successfully prepared.
- A core-sheath flexible conductive fiber with visible light sensing is fabricated.

GRAPHICAL ABSTRACT

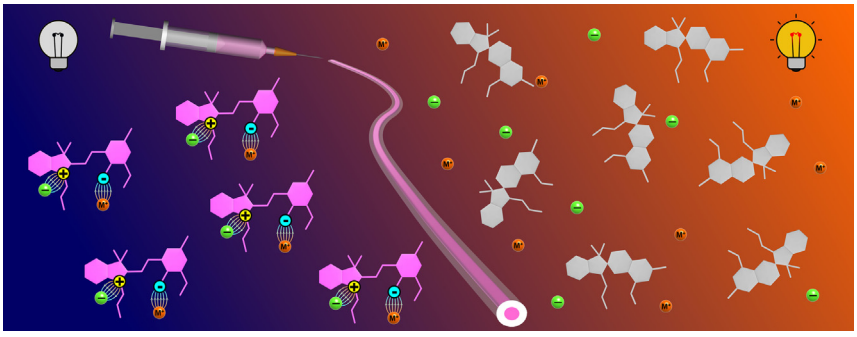

ARTICLE INFO

Article history:
Received 16 February 2023
Revised 31 May 2023
Accepted 1 June 2023
Available online 7 June 2023

Keywords:
Conductive fiber
Visible light sensor
Fibrous sensor
Spiropyran
Merocyanine

ABSTRACT

Flexible conductive fibers have attracted significant attention in the wearable electronics field because of light weight, small size, and easy shape morphing. To date, there are few reports on multifunctional flexible conductive fibers. Finding a facile and effective solution for large-scale production of flexible conductive fibers is still a challenge. In this work, a flexible core-sheath fiber with excellent electrical conductivity (24.71 Ω·m) and visible light sensing is fabricated, which contains a merocyanine diol ($MC(OH)_2$)/$CrCl_3{\cdot}6H_2O$/ethanol aqueous solution core layer and a silicon rubber outer layer. The synthesized $MC(OH)_2$ is an intelligent molecular switch with a visible light response that can reversibly convert from open-form $MC(OH)_2$ to closed-form spiropyran diol ($SP(OH)_2$) after short visible light irradiation. In the reverse process, the transition from $SP(OH)_2$ to $MC(OH)_2$ can occur gradually in the dark. This can be used to sense visible light in addition to electrical conductivity. The reversible change in the electrical resistance of the $MC(OH)_2$/$CrCl_3{\cdot}6H_2O$/ethanol aqueous solution reaches 15.59%. This fiber shows excellent electrical conductivity, good flexibility, a sensitive visible light response, good photochromism, a simple structure, low cost, easy preparation, and suitability for industrial large-scale production, offering promise for applications in the fields of flexible and wearable electronics.

* Corresponding authors.
E-mail addresses: flf880221@163.com (L. Fan), 178323371@qq.com (H. Lu), gf@dhu.edu.cn (F. Gan).

https://doi.org/10.1016/j.matdes.2023.112061
0264-1275/

1. Introduction

Wearable electronics have been widely studied in recent years because of their great application potential in health monitoring [1], gesture recognition [2], wireless communication [3], energy harvesting [4]. Wearable conductors and sensors are important components of wearable electronics [5,6], and should be stretchable, flexible and lightweight. Compared with conventional two-dimensional and three-dimensional wearable conductors and sensors, one-dimensional fibrous wearable conductors and sensors are more popular due to their unique characteristics of light weight, small size, and easy shape morphing [7–11]. Conductive fibers and fibrous sensors can be woven or knitted into textiles that possess excellent stretchability, breathability and high tolerance to damage. Therefore, conductive fibers and fibrous sensors have gained tremendous research interest due to their superior flexibility, high aspect ratio, light weight, small size and high tunability, which enable utilization of conductive fibers and fibrous sensors in a variety of applications, ranging from smart textiles [12] to pressure sensors [13], strain sensors [14], biointerfaces [15] and artificial muscles [16].

The reported conductive fibers can be classified into five categories: metal fibers [17], intrinsically conductive polymer fibers [18], carbon fibers [19], conductive polymer composite fibers [20], and conductive-material-coated fibers [21]. Each kind of conductive fiber has its own shortcomings: metal fibers exhibit a high density, a low strength and susceptibility to corrosion. For intrinsically conductive polymer fibers, the preparation process is difficult, and their conductivity may be lost under certain conditions. Carbon fibers are brittle and not easily bent or woven. The elongation at break of carbon fibers is less than 2%. Conductive polymer composite fibers have low conductivity with increasing length, which is due to the generation of microcracks between the conductive nanomaterials. For conductive-material-coated fibers, the conductive coating easily falls off. Hence, developing a simple, efficient, and mass-production approach for fabricating conductive fibers remains a great challenge.

Spiropyran (SP) and its derivatives [22–29], as a kind of stimuli-responsive photochromic molecular switch, possess a typical bistable molecular structure and usually exhibit positive photochromism in solution. The closed-form SP changes to the open-form zwitterionic merocyanine (MC) upon irradiation with UV light and then returns to the original SP upon exposure to visible light or heat (Fig. 1a). Moreover, this reversible isomerization can be promoted by various other external stimuli, such as temperature [30], acids and bases [31], redox potential [32] and metal ions [33]. The closed-form SP has a ground state energy lower than that of the open-form MC. Due to their stimuli-responsive nature, SP and its derivatives have been extensively researched for use in smart materials [34], data storage [35] and chemical sensors [36].

As open-form MC is a kind of zwitterion, this unique nature attracted our attention. We believe that a solution of zwitterionic MC will possess electrical conductivity, as well as stimulus responsivity. Therefore, MC can be used as a stimulus-responsive electrolyte to prepare conductive fibers in this work. In contrast, the nonionic closed-form SP solution has no electrical conductivity. When exposed to UV light, closed-form SP undergoes a molecular arrangement transformation to open-form MC, and the obtained MC solution has electrical conductivity. The reverse reaction (MC to SP conversion) can be induced by visible light or heat. Therefore, we think that in addition to a reversible color change, the MC solution will also exhibit a reversible change in the electrical conductivity under external stimulation. Hence, an MC solution can be used as an electrical conductor and a UV light sensor.

However, although the above design is feasible in principle, there are still several challenges: ① Most SP and its derivatives usually exhibit positive photochromism in solution (Fig. 1a), and nonionic closed-form SP solutions have no electrical conductivity. External stimulation should be constantly applied to convert SP into MC to make its solution have electrical conductivity, which is not conducive to actual use. ② The common stimulus of SP and its derivatives is UV light, which is weak in penetration and harmful to organisms. ③ As the open-form MC is a kind of zwitterion, the movement of the phenoxy anion and nitrogen cation of $MC(OH)_2$ in the solution is limited, resulting in poor electrical conductivity of the $MC(OH)_2$ solution.

To solve the problem that the positive SP and its derivatives need to be constantly stimulated, we synthesize a negative SP ($MC(OH)_2$) and its molecular structure is shown in Fig. 1b. The designed open-form $MC(OH)_2$ in solution is more stable than the closed-form $SP(OH)_2$. $MC(OH)_2$ is stable in the dark and will transform to closed-form $SP(OH)_2$ after being irradiated by visible light (Fig. 2a and 2b). By introducing an ethanol group onto the benzopyran ring of the designed $MC(OH)_2$, an intramolecular hydrogen bond between the phenate anion and OH group is established (Fig. 1g), which leads to the lower ground state energy of MC $(OH)_2$ compared with $SP(OH)_2$. Therefore, the open-form MC $(OH)_2$ is more stable than $SP(OH)_2$, and the designed $MC(OH)_2$ exhibits negative photochromism because of the intramolecular hydrogen bond. The required stimulus for the reversible transformation between $MC(OH)_2$ and $SP(OH)_2$ is visible light and darkness. Visible light is easy to obtain, does not harm organisms and is environmental friendly in daily use. To solve the problem of poor conductivity of zwitterionic $MC(OH)_2$, we introduce metal salt into the $MC(OH)_2$ solution as an auxiliary electrolyte. Since most metal salts are easily soluble in water and difficult to dissolve in organic solvents, we need to increase the solubility of MC in polar solvents by grafting another hydroxyl group onto the indoline structure of the designed MC molecule so that the synthesized $MC(OH)_2$ can dissolve in the same solvent as various metal salts. Through the above molecular design, we solved all the problems of using SP as a smart electrolyte.

In addition, a variety of $MC(OH)_2$/metal salt/ethanol aqueous solution were prepared, and each solution possessed excellent electrical conductivity and stimulus responsivity to visible light. The reversible change in the electrical resistivity of the prepared solution between visible light and darkness was as high as 15.59%. The prepared $MC(OH)_2$/metal salt/ethanol aqueous solution was used as a conductive medium and injected into a silicone rubber hollow fiber (inner diameter: 0.5 mm, outer diameter: 1 mm) to fabricate a flexible conductive fiber. This flexible conductive fiber was composed of two layers: silicone rubber possessing super elasticity as the outer stretchable fiber layer, and the MC $(OH)_2$/metal salt/ethanol aqueous solution exhibiting excellent electrical performance as the core layer of the conductive fiber. The obtained core-sheath conductive fiber showed excellent electrical performance (24.71 Ω·m) and good tensile properties (354.89% elongation at break). The prepared conductive fiber can reversibly change its electrical resistivity between visible light and dark conditions, as well as its color and fluorescence. Because of the excellent stimulus responsivity to visible light, the fiber can also be used as a flexible fibrous visible light sensor.

In this work, negative SP ($MC(OH)_2$) was first used as an intelligent electrolyte, and a reversible change in the electrical resistance of $MC(OH)_2$ mixed solution was successfully obtained under the stimulation of visible light. A new multifunctional flexible conductive fiber was further manufactured by injecting the prepared MC $(OH)_2$ mixed solution into a silicone rubber hollow fiber. The flex-

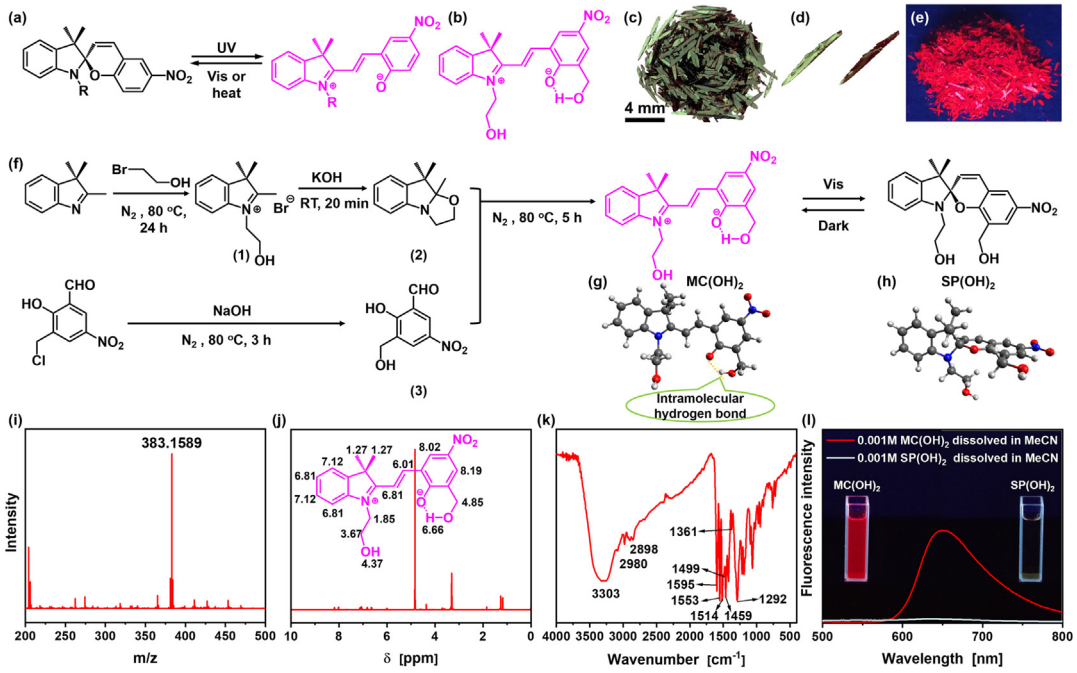

Fig. 1. (a) UV-responsive isomerization between the SP and MC forms of SP derivatives. (b) Structure of the synthesized $MC(OH)_2$. (c) Optical microscopy image of synthesized $MC(OH)_2$ crystals. (d) Optical microscopy images of the same $MC(OH)_2$ crystal observed from different angles. (e) Digital photograph of the fluorescence of $MC(OH)_2$ crystals. (f) Synthesis of $MC(OH)_2$. (g) Geometry-optimized structure of $MC(OH)_2$. (h) Geometry-optimized structure of $SP(OH)_2$. The gray, blue, red and white atoms denote C, N, O, and H atoms, respectively. (i) Mass spectrum of $MC(OH)_2$. (j) ^1H NMR spectra of $MC(OH)_2$. (k) FTIR spectrum of $MC(OH)_2$. (l) Fluorescence spectra of $MC(OH)_2$ and $SP(OH)_2$. (For interpretation of the references to color in this figure legend, the reader is referred to the web version of this article.)

ible conductive fiber based on this design has many advantages compared with other conductive fibers such as good electrical conductivity, a visible light sensing ability, a reversible photochromic ability, a simple structure, low cost, easy preparation, and suitability for industrial large-scale production. Therefore, we provide a new solution for fabricating flexible conductive fibers and visible light sensors in this work. Due to its flexibility and conductivity, the prepared fiber can be applied in the field of wearable electronics; due to its ability to sense visible light, light weight and small size, the produced fiber can be applied to portable electronic devices; and because of its ability to reversibly change color under the stimulation of visible light, this fiber can be applied in the fields of fashion and military.

2. Materials and methods

2.1. Materials

1,3,3-Trimethyl-2-methyleneindoline, 5-nitrosalicylaldehyde, 2,3,3-trimethylindolenine, 2-bromoethanol, 3-chloromethyl-5-nitrosalicylaldehyde, n-hexane sodium hydroxide, ethanol, ethylacetate, acetonitrile, NaCl, $Zn(CH_3COO)_2{\cdot}2H_2O$, $AlCl_3{\cdot}6H_2O$, KCl, $CrCl_3{\cdot}6H_2O$, $CoCl_2{\cdot}6H_2O$, $CdCl_2{\cdot}5/_2H_2O$, $FeCl_3{\cdot}6H_2O$, $SrCl_2{\cdot}6H_2O$, $CuSO_4{\cdot}5H_2O$, $BaCl_2{\cdot}2H_2O$, $MnCl_2{\cdot}4H_2O$, and Na_2SO_4 were purchased from Macklin, China. Unless otherwise stated, all starting materials and reagents were obtained from commercial suppliers and used without further purification.

2.2. Synthesis of 5-hydroxy-1-(2-hydroxyethyl)-2,3,3-trimethyl-3H-indolium bromide (**1**) (Fig. 1f)

2,3,3-Trimethyl-3*H*-indole (2.61 g, 16 mmol) and 2-bromoethanol (2.46 g, 20 mmol) were dissolved in 20 mL of acetonitrile in a flask fitted with a reflux condenser and placed in a preheated 80 °C oil bath under N_2. After being heated for 24 h, acetonitrile and residual 2-bromoethanol were removed by rotary evaporation, and the synthesized product was washed three times with n-hexane to obtain a purple solid with a yield of 70.71%. From the mass spectrum, the exact mass calculated for [M] $C_{13}H_{18}ON$ is 204.31; found: 204.45 (Fig. S1a). Proton nuclear magnetic resonance (^1H NMR, 400 MHz, dimethyl sulfoxide-d6, Fig. S1b): δ (ppm) 1.60, 3.87, 4.60, 7.60, 7.87 and 8.00. The Fourier transform infrared (FTIR) spectrum of the resultant product is shown in Fig. S1c (KBr/cm^{-1}: 3440, 3100, 3060, 3010, 2930, 2870, 1620, 1610, 1480, 1460 and 1090).

2.3. Synthesis of 9,9,9a-trimethyl-2,3,9,9a-tetrahydrooxazolo [3,2-a] indole (**2**) (Fig. 1f)

Compound 1 (2.93 g, 10.00 mmol) and KOH (0.92 g, 16.00 mmol) were added to water and stirred at room temperature for 20 min. The solution was extracted with methyl *tert*-butyl ether (3 × 20 mL). The combined organic layer was dried over Na_2SO_4 and concentrated by evaporation to obtain a yellow oily liquid product with a yield of 80.19%. According to the mass spectrum, the exact mass calculated for $[M + 1]^+$ $C_{13}H_{17}ON$ is 203.28; found: 204.43 (Fig. S1d). ^1H NMR (400 MHz, dimethyl sulfoxide-d6, Fig. S1e): δ (ppm) 1.10, 3.08, 3.46, 3.73, 6.80 and 7.07. The FTIR spectrum of the resultant product is shown in Fig. S1f (KBr/cm^{-1}: 2960, 2880, 1610, 1600, 1480, 1460 and 1080).

2.4. Synthesis of 2-hydroxy-3-(hydroxymethyl)-5-nitrobenzaldehyde (**3**) (Fig. 1f)

3-Chloromethyl-5-nitrosalicylaldehyde (2.00 g, 9.27 mmol) and NaOH (3 mL, 3 mol/L) were added to water (2 mL) and stirred at 80 °C under N_2 for 3 h. The solvent was removed by rotary evaporation, and the obtained product was recrystallized three times in water to obtain a yellow-green powder with a yield of 79.52%. Based on the mass spectrum, the exact mass calculated for

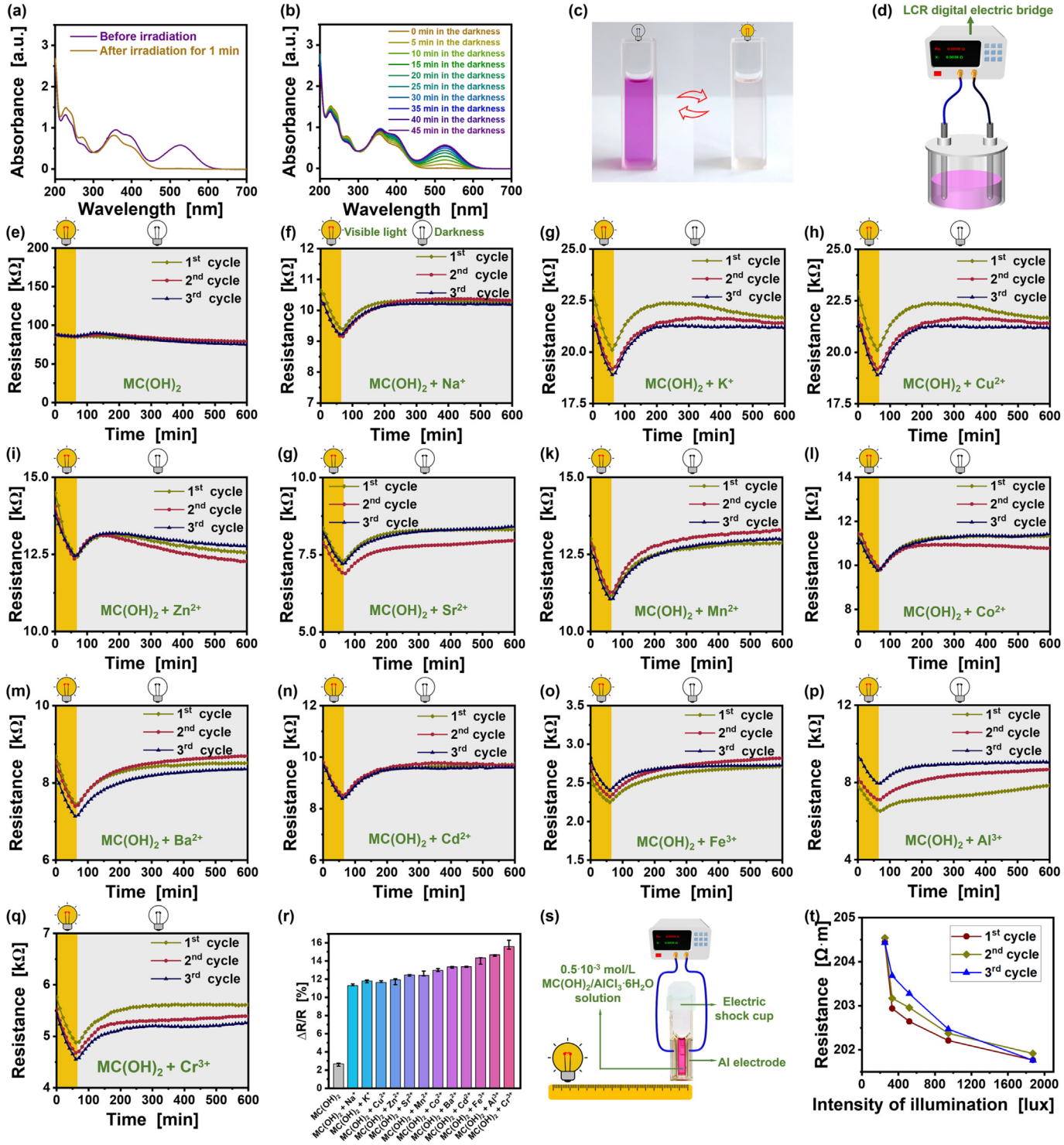

Fig. 2. (a) UV–vis spectra of $MC(OH)_2$ (1 mM) in a EtOH-water (v:v = 1:1) mixture after visible light irradiation (~1800 lx). (b) UV–vis spectra of $SP(OH)_2$ (1 mM) in a EtOH-water (v:v = 1:1) mixture in the dark. (c) Reversible color change of $MC(OH)_2$ after visible light irradiation/sitting in the dark. (d) Setup for recording the electrical resistance of the $MC(OH)_2$ mixed solution. (e-q) Electrical resistance of $MC(OH)_2$/various metal salts (0.5 mM, 0.5 mM) in EtOH-water (v:v = 1:1) mixed solutions during three visible light irradiation (1 h) and darkness (9 h) cycles. (r) Reversible change in the electrical resistance of $MC(OH)_2$/various metal salts in EtOH-water (v:v = 1:1) mixed solutions. (s) Setup of the visible light sensor. (t) Correspondence between visible light intensity and electrical conductivity of $MC(OH)_2/AlCl_3{\cdot}6H_2O$ (0.5 mM, 0.5 mM) in a EtOH-water (v:v = 1: 1) mixed solution.

$[M-1]^-$ $C_8H_7NO_5$ is 197.15; found: 196.21 (Fig. S1g). ^1H NMR (400 MHz, dimethyl sulfoxide-d6, Fig. S1h): δ (ppm) 4.61, 8.13, 8.33, 8.44, 8.58 and 8.77. The FTIR spectrum of the resultant product is shown in Fig. S1i (KBr/cm^{-1}: 3210, 2870, 1660, 1620, 1590, 1520, 1450 and 1350).

*2.5. Synthesis of 2-{(E)-[1-(2-hydroxyethyl)-3,3-dimethyl-3H-indol-1-ium-2-yl]vinyl}-6-hydroxymethyl-4-nitrophenolate (**MC(OH)$_2$**)*

Compound 2 (1.00 g, 4.90 mmol) and compound 3 (0.81 g, 4.10 mmol) were added to a 50% ethanol aqueous solution (v/v)

(14 mL) and stirred at 80 °C for 5 h under N_2. The solvent was removed by rotary evaporation, and the obtained product is recrystallized three times in 14 mL of a 70% MeCN aqueous solution (v/v) to obtain purple crystals with a yield of 69.60%. From the mass spectrum, the exact mass calculated for $[M + 1]^+$ $C_{21}H_{22}N_2O_5$ is 382; found: 383.1589 (Fig. 1i). ^{1}H NMR (400 MHz, MeOD, Fig. 1j): δ (ppm) 1.27, 1.85, 3.67, 4.37, 4.85, 6.01, 6.66, 6.81, 7.12, 8.02, 8.19. The FTIR spectrum of the resultant product is shown in Fig. 1k (KBr/cm^{-1}: 3303, 2980, 2898, 1595, 1553, 1514, 1499, 1459, 1361 and 1292).

2.6. Preparation of the visible light sensor

A 1×10^{-3} mol/L $AlCl_3{\cdot}6H_2O$ EtOH aqueous solution (v:v = 1:1, 10 mL) and a 1×10^{-3} mol/L $MC(OH)_2$ EtOH aqueous solution (v:v = 1:1, 10 mL) were added into a beaker and stirred at room temperature for 10 min to obtain the conductive mixed solution. The prepared conductive solution (0.05 mL) was added to micropulser electroporation cuvettes (Fig. 2s) to obtain a visible light sensor, and the gap between the two aluminum electrode plates of the micropulser electroporation cuvettes was 4 mm.

2.7. Preparation of the flexible conductive fiber

A 0.1 M $CrCl_3{\cdot}6H_2O$ EtOH aqueous solution (v:v = 1:1, 10 mL) and a 0.1 M $MC(OH)_2$ EtOH aqueous solution (v:v = 1:1, 10 mL) were added into a beaker and stirred at room temperature for 10 min to obtain the conductive mixed solution.The prepared conductive solution was injected into a flexible silicone hollow fiber (external diameter: 1.0 mm, internal diameter: 0.5 mm) to yield the flexible conductive fiber.

2.8. Characterization

Mass spectra were collected using a mass spectrometer (Thermo Fisher Corporation, US). FTIR were recorded by a Nicolet Is50 spectrometer (Thermo, US). ^{1}H NMR spectra were collected by means of an AVANCE III (400 MHz, Bruker, Germany) with dimethyl sulfoxide-d6 or MeOD as the solvent. Fluorescence spectra were measured using a spectrophotometer (RF-6000, Shimadzu, Japan). Fluorescence spectra measurements were carried out at an excitation wavelength of 467 nm. Absorption spectra were measured using a 10 mm path length quartz cell on an UV–vis spectrophotometer (UV-6100, Shanghai Yuanxi Instruments, China) equipped with a temperature controller. Visible light irradiation was carried out with an LED lamp (18 W, Eryuehe Lighting Co., Ltd., China). The visible light intensity was measured with a digital illuminometer (TA9130, Suzhou Tiansi Electronics Co., Ltd., China). The light intensity was tuned by changing the distance between the LED lamp and the sample. The surface morphologies of the synthesized $MC(OH)_2$ crystals were characterized by optical microscopy (VHX-6000, KEYENCE, Japan). Tensile tests were conducted on a universal tester (Shenzhen Rambo Sansi Material Testing Co., Ltd., China) at a crosshead speed of 50 mm/min at 25 °C. All electrical conductivity measurements were taken using an LCR digital bridge (4091C, Shengli Instruments, Co., Ltd., China). The voltage was measured by a digital multimeter (17B+, Fluke, US).

3. Results

3.1. Characterization of $MC(OH)_2$

The FTIR spectrum of the synthesized $MC(OH)_2$ is given in Fig. 1k. The peak appearing at 3303 cm^{-1} is attributed to the stretching vibration of the hydroxyl group (–OH) of $MC(OH)_2$. The peaks at 2980 cm^{-1} and 2898 cm^{-1} correspond to the stretching vibration of carbon-hydrogen bonds (-C–H) of methyl (–CH_3) in the $MC(OH)_2$ structure. The peaks found at 1514 cm^{-1} and 1361 cm^{-1} prove the existence of the nitro group (–NO_2), and that at 1292 cm^{-1} should be the stretching vibration peak of C-N. The bending vibration peaks appearing at 1595 cm^{-1}, 1553 cm^{-1}, 1499 cm^{-1} and 1292 cm^{-1} can be ascribed to the vibration of the aromatic ring. The FTIR spectrum indicates that OH has been successfully introduced into $MC(OH)_2$. According to the ^{1}H NMR spectrum (MEOD, δ ppm) of $MC(OH)_2$ (Fig. 1j), the peaks at 6.66 ppm and 4.37 ppm are the chemical shifts of OH, which proves that the product has been successfully synthesized as designed. The same conclusion was obtained from another angle based on the mass spectrum. In the MS spectrum (Fig. 1i), the peak at m/z = 383.1589 corresponds to the $[M + H]^+$ species. An optical microscopic image of the synthesized $MC(OH)_2$ crystals is shown in Fig. 1c. The synthesized $MC(OH)_2$ crystals have obvious metallic luster (Fig. 1c). The same crystal shows different colors when observed from different angles (Fig. 1d). The synthesized $MC(OH)_2$ crystals can produce bright purple–red fluorescence after being irradiated by ultraviolet light (Fig. 1e) as can the $MC(OH)_2$ solution (Fig. 1l). After being irradiated by visible light, $MC(OH)_2$ dissolved in MeCN transforms into $SP(OH)_2$ through molecular arrangement. The color of the solution changes from purple to colorless (Fig. 2c), and no fluorescence can be observed when the solution is irradiated by ultraviolet light (Fig. 1l). When the colorless solution is placed in the dark, it gradually becomes purple, which means that $SP(OH)_2$ transforms into $MC(OH)_2$ through molecular rearrangement again.

To confirm that the synthesized $MC(OH)_2$ possesses negative reversible photochromism in solution, UV–vis spectral analysis was carried out. Fig. 2a shows the time-dependent change in the absorption spectra of $MC(OH)_2$ (0.05 mM) in a water-EtOH (v:v = 1:1) mixture at room temperature under visible light irradiation (~1800 lx). At 0 min, an obvious absorption band appears at 440–640 nm, with a maximum absorption at 527 nm, which indicates that the obtained product exists in the open form. However, as time advances to 1 min, no absorption appears at > 470 nm, and the color of the mixed solution changes from purple to colorless, indicating that the synthesized product exists in the closed form. In the reverse process, when the mixed solution is placed in dark conditions, the transition from closed-form $SP(OH)_2$ to open-form $SP(OH)_2$ gradually occurs as shown in Fig. 2b. With increasing time, the intensity of the absorption band at 527 nm gradually increases. After 45 min, the absorption band appearing at 440–640 nm returns to its original position. Therefore, we believe that the closed-form $SP(OH)_2$ will completely transform to the open-form $MC(OH)_2$ after 45 mins under dark conditions. Based on the above analysis, we can conclude that the synthesized $MC(OH)_2$ is stable in the open form under dark conditions and will quickly change to the closed-form $SP(OH)_2$ after visible light irradiation. The above results also prove that the transformation between $MC(OH)_2$ and $SP(OH)_2$ is reversible.

Why does the synthesized product $MC(OH)_2$ possess negative photochromism in solution? We think that this is due to the unique molecular structure of $MC(OH)_2$. As shown in Fig. 1g, an intramolecular hydrogen bond has been established between the ethanol group and the oxygen atom of the phenoxy anion, which increases the stability of the open-form $MC(OH)_2$. To verify the above assumption, the geometries and Gibbs free energies (G) of $MC(OH)_2$ and $SP(OH)_2$ were optimized with the ORCA version 5.0.3 program [37–42], which is an ab initio density functional theory (DFT) semiempirical SCF-MO package, using the r2SCAN-3c computing method in this work. According to the experimental results of the ORCA program, $\Delta G = G_{MC(OH)_2} - G_{SP(OH)_2}$ = –32.07 kJ·mol

$^{-1}$. Due to the lower Gibbs free energy, $MC(OH)_2$ is more stable than $SP(OH)_2$. ΔG = –32.07 kJ·mol^{-1} matches the bond energy of moderate hydrogen bonds (15 to 60 kJ/mol [43]). Based on the above analysis, the formation of intramolecular hydrogen bond makes open-form $MC(OH)_2$ have a lower ground state energy, which is the main reason why $MC(OH)_2$ is more stable than $SP(OH)_2$.

3.2. Use of $MC(OH)_2$ as a smart electrolyte

As the synthesized $MC(OH)_2$ is a kind of zwitterion (Fig. 1b), its solution should possess electrical conductivity. Hence, $MC(OH)_2$ can be used as an electrolyte and visible light sensor because it can change from the open-form $MC(OH)_2$ to the closed-form $SP(OH)_2$ under the stimulation of visible light, resulting in reversible changes in the electrical conductivity and color of the mixed solution. To verify the abovementioned function, $MC(OH)_2$ was dissolved in an ethanol aqueous solution (v: v = 1:1) at a concentration of 1 mM, and the electrical conductivity of the prepared mixed solution was measured in the dark at room temperature. As shown in Fig. 2d, the prepared mixed solution (20 mL) was added to an electrolytic cell, and the resistance of the mixed solution between the two graphite electrodes was tested by the LCR digital bridge. According to Fig. 2e, the electrical resistance of the prepared solution in the dark is 86.60 kΩ, which proves that the solution of $MC(OH)_2$ is conductive and that $MC(OH)_2$ can be used as an electrolyte. When the system is exposed to visible light (~1800 lx), $MC(OH)_2$ in the mixed solution transforms into $SP(OH)_2$ and the color of the solution changes from purple to colorless.

Based on the mutual attraction between anions and cations, the phenoxy anion of $MC(OH)_2$ will generate electrostatic attraction for the tiny amount of H^+ produced by ionization of water, and the nitrogen cation of $MC(OH)_2$ will generate electrostatic attraction for the tiny amount of OH^- produced by ionization of water. Therefore, $MC(OH)_2$ will reduce the motion speed of H^+ and OH^-. When the mixed solution is exposed to visible light, $MC(OH)_2$ will be converted into $SP(OH)_2$, and thus, the electrostatic attraction between $MC(OH)_2$ and H^+ and OH^- will disappear, and the influence on the movement speed of H^+ and OH^- in the solution will be lost, further leading to a decrease in the electrical resistance of the system. When the mixed solution is placed in the dark, the closed-form $SP(OH)_2$ will change back to the open-form $MC(OH)_2$, the electrostatic attraction between $MC(OH)_2$ and H^+ and OH^- will reappear, and the influence on the movement speed of H^+ and OH^- will gradually recover, further leading to a gradual increase in the electrical resistance of the system.

According to Fig. 2e, the electrical conductivity of the $MC(OH)_2$ solution is very weak because the phenoxy anion and nitrogen cation are simultaneously connected on the $MC(OH)_2$ molecule, and the reversible change in the electrical resistivity of the MC $(OH)_2$ solution is only 2.68%. To increase the electrical conductivity of the $MC(OH)_2$ solution, equi molar metal salts were introduced into the system as auxiliary electrolytes. Therefore, various metal salt/$MC(OH)_2$ solutions were prepared as follows. A stock solution of $MC(OH)_2$ (1 mM) was prepared by dissolving $MC(OH)_2$ in an ethanol aqueous solution (v:v = 1:1). Stock solutions of various metal salts was prepared by dissolving the corresponding metal salts in ethanol aqueous solution (v:v = 1:1). The test solution was prepared by mixing the selected metal salt solution (50 mL) with the stock solution of $MC(OH)_2$ (50 mL). The different metal salt/$MC(OH)_2$ solutions were added to the electrolytic cell, and the electrical resistance of the mixed solution between the two graphite electrodes was measured by the LCR digital bridge (Fig. 2d). According to Fig. 2f-2q, the electrical resistance of the different metal salt/$MC(OH)_2$ solutions is much lower than that of the pure $MC(OH)_2$ solution due to the introduction of metal salts, and the average electrical resistivity of the mixed solution is reduced from 86.60 kΩ to 11.15 kΩ.

Since the phenoxy anion on SP and its derivatives provides the possibility for coordination with metal ions, SP and its derivatives can be used to detect metal ions [44]. In this work, if metal ions are coordinated with the synthesized $MC(OH)_2$, then the electrical conductivity of the mixed solution will be significantly reduced. Therefore, UV–vis spectra (Fig. S2), FTIR spectra (Fig. S3) and MS spectra (Fig. S4) were used to characterize whether $MC(OH)_2$ coordinates with the selected metal ions (Na^+, K^+, Cu^{2+}, Zn^{2+}, Sr^{2+}, Mn^{2+}, Co^{2+}, Ba^{2+}, Cd^{2+}, Fe^{3+}, Al^{3+}, Cr^{3+}). No peak shift was observed in the UV–vis spectra (Fig. S2) and FTIR spectra (Fig. S3), and no molecular ion peak of coordination compounds was found in the mass spectrum (Fig. S4). According to the above experimental results, we believe that $MC(OH)_2$ cannot coordinate with the selected metal ions.

In addition to reducing the electrical resistivity of the $MC(OH)_2$ solution, the introduction of metal salts has another important function, i.e., significantly improving the reversible change in the electrical conductivity of the mixed solution between visible light stimulation and in the dark. After visible light irradiation, MC $(OH)_2$ in the mixed solution is in a closed form ($SP(OH)_2$). The conductivity of the mixed solution is contributed by metal salts; when the mixed solution is placed in the dark, the closed-form $SP(OH)_2$ will gradually convert into the zwitterionic open form (MC $(OH)_2$). At this time, the metal salts and $MC(OH)_2$ zwitterion contribute to the electrical conductivity of the mixed solution. Theoretically, the electrical conductivity of the mixed solution will increase due to the aid of the $MC(OH)_2$ zwitterion. However, to our surprise, the electrical conductivity of the mixed solution significantly decreases. As shown in Fig. 2f-2q, the electrical resistivity increased in the dark condition. When the mixed solution is placed in the dark, the closed-form $SP(OH)_2$ will gradually convert into the zwitterionic open form ($MC(OH)_2$). The phenoxy anion and nitrogen cation of $MC(OH)_2$ will generate electrostatic attraction for the metal ions and acid radicals, respectively, and the movement speed of metal ions and acid radicals in the mixed solution obviously decreases, which leads to an increase in the electrical resistance of the mixed solution. When the mixed solution is exposed to visible light again, $MC(OH)_2$ will be converted into SP $(OH)_2$, and thus, the electrostatic attraction between $MC(OH)_2$ and metal ions and acid radicals will disappear, and the influence on the movement speed of metal ions and acid radicals in the solution will be lost, further leading to a decrease in the electrical resistance of the mixed solution. Therefore, under the stimulation of visible light irradiation/darkness, the electrical resistance of the prepared mixed solution can be reversibly reduced/increased.

Fig. 2r shows that with the increase in the valence of the selected metal ions, the reversibility of the electrical resistance $\Delta R/R$ of the mixed solution is improved. The average $\Delta R/R$ values of the mixed solutions containing equimolar monovalent metal ions, divalent metal ions and trivalent metal ions are 11.55%, 12.70% and 14.82% (Fig. 2r), respectively. When the added metal salt is $CrCl_3{\cdot}6H_2O$, the maximum reversible electrical resistance change of the mixed solution is as high as 15.59%. To highlight the function of $MC(OH)_2$, we also measured the electrical resistance change of pure metal salt solution under visible light stimulation/dark conditions. As shown in Fig. S5, the resistance of the metal salt solution remains unchanged when it is irradiated by visible light. Therefore, we believe that the reversible change in electrical resistance of the $MC(OH)_2$/metal salt ethanol aqueous solution under visible light stimulation/darkness is contributed by of $MC(OH)_2$.

3.3. Visible light sensor

We prepared a visible light sensor utilizing the nature of the prepared $MC(OH)_2/AlCl_3{\cdot}6H_2O$ ethanol aqueous solution as shown

in Fig. 2s. The visible light sensor is composed of an electric shock cup (Fig. 2s) and the prepared mixed solution. The electric shock cup is equipped with embedded aluminum electrodes (Fig. 2s), and the gap between the electrodes is 4 mm. Except for the electrodes, the other parts of the electric shock cup are made of colorless transparent plastic, so it has good visible light transmission. The visible light sensor is made by simply adding 0.05 mL of the prepared mixed solution into the electric shock cup. The prepared visible light sensor was connected to the LCR digital bridge through wires. By measuring the electrical resistance of the mixed solution in the electric shock cup, the visible light intensity at the location of the prepared visible light sensor can be deduced. The visible light intensity at the position of the obtained visible light sensor was adjusted by changing the distance between the LED lamp and the sensor. The specific circuit diagram is shown in Fig. 2s. The distance was reduced by 10 cm every 20 mins to realize a gradual increase in the visible light intensity. As shown in Fig. 2t, as the distance decreases, the illumination at the location of the visible light sensor gradually increases from 251.33 lx to 1874.00 lx, and the electrical conductivity of the prepared visible light sensor decreases from 204.47 Ω·m to 201.82 Ω·m. The above experiment was repeated three times and similar results were obtained (Fig. 2t).

3.4. Conductive fiber

In addition to a visible light sensor, the prepared mixed solution is utilized to manufacture flexible conductive fibers. As shown in Fig. 3a, the prepared 0.5 mM $MC(OH)_2/CrCl_3{\cdot}6H_2O$ ethanol aqueous solution was injected into a silicone hollow fiber (inner diameter: 0.5 mm, outer diameter: 1 mm) to prepare a conductive fiber with a core-sheath structure. As the material selected for the outer layer of the conductive fiber is silicone rubber, it possesses excellent flexibility and elasticity. The tensile strength and elongation at break of the silicone rubber are 8.24 MPa and 354.89% (Fig. 3b), respectively. Because the 0.5 mM $MC(OH)_2/CrCl_3{\cdot}6H_2O$ ethanol aqueous solution as a conductive medium has good fluidity, it will not affect the mechanical properties of the silicone hollow fiber, so the prepared conductive fiber simultaneously has good conductivity and flexibility at the same time. Moreover, the selected silicone hollow fiber is transparent, and the visible light transmittance of the silicone hollow fiber is as high as 88% (Fig. S6). Therefore, the prepared flexible conductive fiber also has photochromic ability, and it can be used as a fibrous visible light sensor.

To characterize the electrical conductivity of the prepared conductive fiber, both ends of the conductive fiber were connected to the LCR digital bridge. According to Fig. S7, the electrical conductivity of the obtained fiber decreases as the concentration of the mixed solution increases. When the concentration of the mixed solution was 0.05 M, the electrical conductivity of the fiber is as high as 24.71 Ω·m. Even when the concentration of the mixed solution is as low as $5{\cdot}10^{-4}$ M, the obtained fiber still has good conductivity (514.38 Ω·m). After visible light (~1800 lx) irradiation for 1 min, the electrical conductivity of the fiber decreases from 24.71 Ω·m to 22.70 Ω·m, and the fiber color changes from purple to colorless. Based on the above experimental results, the prepared fiber has excellent electrical conductivity, good flexibility, a sensitive visible light response, and good photochromism.

Both ends of the selected flexible conductive fiber were connected to an LED bulb and an adjustable DC power supply through wires as shown in Fig. 3**e**. The voltage of the DC power supply is adjusted to make the voltage applied to the LED bulb 2.30 V, which

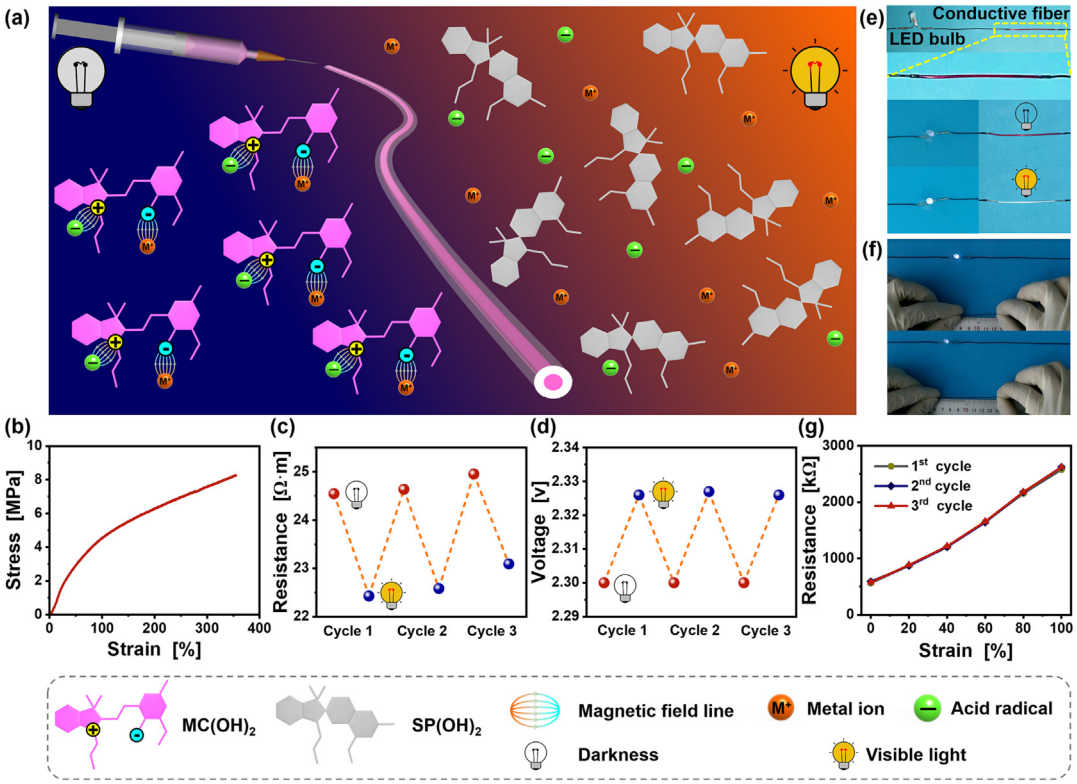

Fig. 3. (a) Conceptual design of the flexible multifunctional conductive fiber. (b) Typical tensile stress–strain curve of the silicone hollow fiber. (c) Electrical conductivity of the $MC(OH)_2/CrCl_3{\cdot}6H_2O$ (0.05 M, 0.05 M) ethanol aqueous solution during three visible light irradiation (2 min) and darkness (45 min) cycles. (d) Voltage applied to the LED bulb during three visible light irradiation (2 min) and darkness (45 min) cycles. (e) Brightness of the LED bulb controlled by the prepared conductive fiber in response to the visible light intensity. (f) Prepared conductive fiber with a 45 mm original length (above) and stretched to 74 mm (below). (g) Electrical resistance of the prepared conductive fiber as a function of strain.

is higher than its turn-on voltage, and the bulb illuminates. As the fiber is placed in the dark, the $MC(OH)_2$ in the mixed solution remains in the open form. Therefore, the phenoxy anion and nitrogen cation of $MC(OH)_2$ reduce the movement speed of Cr^{3+} and Cl^-. Under visible light (~1800 lx) irradiation, the $MC(OH)_2$ in the mixed solution inside the silicone hollow fiber is in the closed form, so the color of the fiber is colorless, and the movement of Cr^{3+} and Cl^- is free and not affected by the phenoxy anion and nitrogen cation of the open-form $MC(OH)_2$. This leads to a decrease in the electrical resistance of the fiber, and the voltage applied to the LED bulb increases from 2.30 V to 2.33 V, which causes the brightness of the LED bulb to increase. When the visible light is removed and the fiber is placed in the dark again, the color of the fiber turns purple and the LED bulb darkens again. Therefore, the visible light can be directly indicated by the brightness of the LED bulb.

To prove the flexibility of the prepared core-sheath fiber from other angles, the change in its electrical resistance under tensile deformation was recorded. The obtained conductive fiber was stretched to 0%, 20%, 40%, 60%, 80%, and 100%, and the electrical resistance at different strains was measured by the LCR digital bridge, as shown in Fig. 3g. When the fiber is stretched to 65%, the brightness of the LED significantly decreases (Fig. 3f) due to the reduction in the cross-sectional area of the fiber core. Therefore, the fiber can also be used as a strain sensor.

The prepared flexible conductive fiber can not only be added into fabric to prepare wearable electronics, but can also be used to prepare a variety of visible light sensors through traditional textile technology. As shown in Fig. 4a-4c, imitating roses (Fig. 4a) in nature, the obtained conductive fibers are utilized to prepare an artificial rosette visible light sensor (Fig. 4b**)** through embroidery. In addition to sensing visible light, the prepared rose can also exhibit color changes under different visible light intensities and show charming colors (Fig. 4c) under ultraviolet radiation. Therefore, it is a multifunctional sensor that integrates beauty, decoration and the function of sensing visible light. Similarly, by imitating a bracelet (Fig. 4d) and a Chinese knot (Fig. 4g), a bracelet (Fig. 4e) and a Chinese knot brooch (Fig. 4h) with the function of visible light sensing were made by weaving the fibers. The above products not only have their own decorative functions, but can also sense visible light and show amazing colors (Fig. 4f and 4i) under ultraviolet radiation.

4. Conclusions

In this work, we have successfully synthesized merocyanine diol, which exhibits negative photochromism in solution. The synthesized $MC(OH)_2$ is an intelligent molecular switch with a visible light response. It is stable in the dark and will quickly transform into the closed-form $SP(OH)_2$ after being irradiated by visible light; in contrast, the closed-form $SP(OH)_2$ will gradually change back to the open-form $MC(OH)_2$ in the dark. As the synthesized $MC(OH)_2$ is a kind of zwitterion, its solution possesses electrical conductivity and can be used as an electrolyte. To increase the electrical conductivity of the $MC(OH)_2$ solution, equi molar metal salts were introduced into the system as auxiliary electrolytes. The maximum

Fig. 4. (a) Digital photograph of a purple rose. (b) Artificial rose made of the prepared conductive fibers through embroidery. (c) Digital photograph of the fluorescence of the artificial rose. (d) Digital photograph of a bracelet. (e) Bracelet made of the prepared conductive fibers through knitting. (f) Digital photograph of the fluorescence of the obtained bracelet. (g) Digital photograph of a Chinese knot. (h) Chinese knot made of the prepared conductive fibers through knitting. (i) Digital photograph of the fluorescence of the obtained Chinese knot. (For interpretation of the references to color in this figure legend, the reader is referred to the web version of this article.)

reversible change in the electrical resistance of the $MC(OH)_2/CrCl_3 \cdot 6H_2O$/ethanol aqueous solution is as high as 15.59%.

A flexible conductive fiber with a core-sheath structure was obtained by injecting the $MC(OH)_2/CrCl_3 \cdot 6H_2O$/ethanol aqueous solution into a flexible silicone hollow fiber. The $MC(OH)_2/CrCl_3 \cdot 6H_2O$/ethanol aqueous solution in the core layer provides the fiber with good electrical conductivity (24.71 Ω·m), a visible light sensing ability and a photochromic ability, while silicone rubber at the outer sheath layer provides the fiber with sufficient flexibility, light transmission and weather resistance. Therefore, the combination of the two layers makes the fiber a multifunctional and high-performance smart fiber. It has multiple advantages compared with other conductive fibers, such as good electrical conductivity, a visible light sensing ability, and reversible photochromic ability, as well as a simple structure, low cost, easy preparation, and suitability for industrial large-scale production.

Data availability

Data will be made available on request.

Declaration of Competing Interest

The authors declare that they have no known competing financial interests or personal relationships that could have appeared to influence the work reported in this paper.

Acknowledgment

The authors thank the support of the National Natural Science Foundation of China (Grants: 52003201 and 52103010), Guangdong Basic and Applied Basic Research Foundation (Grants: 2019A1515110327 and 2020A1515110897), the Natural Science Foundation of Guangdong Province, China (Grant: 2023A1515010694), Joint Research Fund for Wuyi University, Hong Kong and Macao Young Scholars (Grant: 2019WGALH05), Basic and Applied Basic Research Foundation of Jiangmen (Grant: 2021030102790006114), Science Foundation for Young Teachers of Wuyi University (Grant: 2018AL017), and Bureau of Science and Technology of Jiangmen Municipality (Grant: 2021030102030004890).

Appendix A. Supplementary data

Supplementary data to this article can be found online at https://doi.org/10.1016/j.matdes.2023.112061.

References

[1] Y. Niu, H. Liu, R. He, Z. Li, H. Ren, B. Gao, H. Guo, G.M. Genin, F. Xu, The new generation of soft and wearable electronics for health monitoring in varying environment: From normal to extreme conditions, Mater. Today 41 (2020) 219–242, https://doi.org/10.1016/j.mattod.2020.10.004.

[2] L. Yan, Y. Mi, Y. Lu, Q. Qin, X. Wang, J. Meng, F. Liu, N. Wang, X. Cao, Weaved piezoresistive triboelectric nanogenerator for human motion monitoring and gesture recognition, Nano Energy 96 (2022), https://doi.org/10.1016/j.nanoen.2022.107135 107135.

[3] K. Chang, M. Guo, L. Pu, J. Dong, L.e. Li, P. Ma, Y. Huang, T. Liu, Wearable nanofibrous tactile sensors with fast response and wireless communication, Chem. Eng. J. 451 (2023) 138578.

[4] M. Li, B. Xu, Z. Li, Y. Gao, Y. Yang, X. Huang, Toward 3D double-electrode textile triboelectric nanogenerators for wearable biomechanical energy harvesting and sensing, Chem. Eng. J. 450 (2022), https://doi.org/10.1016/j.cej.2022.137491 137491.

[5] C. Zhang, M. Wang, C. Jiang, P. Zhu, B. Sun, Q. Gao, C. Gao, R. Liu, Highly adhesive and self-healing γ-PGA/PEDOT:PSS conductive hydrogels enabled by multiple hydrogen bonding for wearable electronics, Nano Energy 95 (2022), https://doi.org/10.1016/j.nanoen.2022.106991 106991.

[6] G. Luo, J. Xie, J. Liu, Q. Zhang, Y. Luo, M. Li, W. Zhou, K. Chen, Z. Li, P. Yang, L. Zhao, K.S. Teh, X. Wang, L. Dong, R. Maeda, Z. Jiang, Highly conductive, stretchable, durable, breathable electrodes based on electrospun polyurethane mats superficially decorated with carbon nanotubes for multifunctional wearable electronics, Chem. Eng. J. 451 (2023), https://doi.org/10.1016/j.cej.2022.138549 138549.

[7] L. Wang, X. Fu, J. He, X. Shi, T. Chen, P. Chen, B. Wang, H. Peng, Application challenges in fiber and textile electronics, Adv. Mater. 32 (2020) 1901971, https://doi.org/10.1002/adma.201901971.

[8] D. Malka, A four green TM/Red TE demultiplexer based on multi slot-waveguide structures, Materials 13 (2020) 3219, https://doi.org/10.3390/ma13143219.

[9] E. Cohen, D. Malka, A. Shemer, A. Shahmoon, Z. Zalevsky, M. London, Neural networks within multi-core optic fibers, Sci. Rep.-UK 6 (2016) 29080, https://doi.org/10.1038/srep29080.

[10] X. Chen, F. Wang, L. Shu, X. Tao, L. Wei, X. Xu, Q. Zeng, G. Huang, A single-material-printed, low-cost design for a carbon-based fabric strain sensor, Mater. Design 217 (2022), https://doi.org/10.1016/j.matdes.2022.110926 110606.

[11] R. Yu, A. Senocrate, F. Bernasconi, T. Künniger, L. Müller, R. Pauer, C. Battaglia, X. Wang, J. Wang, Flexible and ultrathin waterproof conductive cellular membranes based on conformally gold-coated PVDF nanofibers and their potential as gas diffusion electrode, Mater. Design 225 (2023), https://doi.org/10.1016/j.matdes.2022.111441 111441.

[12] Y. Wu, X. Dai, Z. Sun, S. Zhu, L. Xiong, Q. Liang, M.-C. Wong, L.-B. Huang, Q. Qin, J. Hao, Highly integrated, scalable manufacturing and stretchable conductive core/shell fibers for strain sensing and self-powered smart textiles, Nano Energy 98 (2022), https://doi.org/10.1016/j.nanoen.2022.107240 107240.

[13] Y. Wang, Y. Yue, F. Cheng, Y. Cheng, B. Ge, N. Liu, Y. Gao, $Ti_3C_2T_x$ MXene-based flexible piezoresistive physical sensors, ACS Nano 16 (2022) 1734–1758, https://doi.org/10.1021/acsnano.1c09925.

[14] S. Yang, W. Yang, R. Yin, H. Liu, H. Sun, C. Pan, C. Liu, C. Shen, Waterproof conductive fiber with microcracked synergistic conductive layer for high-performance tunable wearable strain sensor, Chem. Eng. J. 453 (2023), https://doi.org/10.1016/j.cej.2022.139716 139716.

[15] Z. Hussain, P.i. Ding, L. Zhang, Y. Zhang, S. Ullah, Y. Liu, I. Ullah, Z. Wang, P. Zheng, R. Pei, Multifaceted tannin crosslinked bioinspired dECM decorated nanofibers modulating cell-scaffold biointerface for tympanic membrane perforation bioengineering, Biomed. Mater. 17 (3) (2022) 034102.

[16] C. Fu, K. Wang, W. Tang, A. Nilghaz, C. Hurren, X. Wang, W. Xu, B. Su, Z. Xia, Multi-sensorized pneumatic artificial muscle yarns, Chem. Eng. J. 446 (2022), https://doi.org/10.1016/j.cej.2022.137241 137241.

[17] J.S. Sun, H.S. Gokturk, D.M. Kalyon, Volume and surface resistivity of low-density polyethylene filled with stainless steel fibers, J. Mater. Sci. 28 (1993) 364–366, https://doi.org/10.1007/bf00357809.

[18] E. Tavakkol, H. Tavanai, A. Abdolmaleki, M. Morshed, Production of conductive electrospun polypyrrole/poly(vinyl pyrrolidone) nanofibers, Synth Met 31 (2017), https://doi.org/10.1016/j.synthmet.2017.06.017.

[19] M.E. Kozlov, R.C. Capps, W.M. Sampson, V.H. Ebron, J.P. Ferraris, R.H. Baughman, Spinning solid and hollow polymer-free carbon nanotube fibers, Adv. Mater. 17 (2005) 614–617, https://doi.org/10.1002/adma.200401130.

[20] Y. Wang, J. Yang, S. Zhou, W. Zhang, R. Chuan, Electrical properties of graphene nanoplatelets/ultra-high molecular weight polyethylene composites, J. Mater. Sci.-Mater. El. 29 (2018) 91–96, https://doi.org/10.1007/s10854-017-7892-4.

[21] D. Zabetakis, M. Dinderman, P. Schoen, Metal-coated cellulose fibers for use in composites applicable to microwave technology, Adv. Mater. 17 (2005) 734–738, https://doi.org/10.1002/adma.200400320.

[22] F. Liu, K. Morokuma, Multiple pathways for the primary step of the spiropyran photochromic reaction: a CASPT2//CASSCF study, J. Am. Chem. Soc. 135 (2013) 10693–10702, https://doi.org/10.1021/ja402868b.

[23] E.A. Yurieva, S.M. Aldoshin, Spiropyran salts and their neutral precursors: synthesis, crystal structure, photochromic transformations in solutions and solid state, Org. Photonics Photovolt. 3 (2015) 42–53, https://doi.org/10.1515/oph-2015-0004.

[24] Y. Funasako, A. Takaki, M. Inokuchi, T. Mochida, Photo-, thermo-, and piezochromic nafion film incorporating cationic spiropyran, Chem. Lett. 45 (2016) 1397–1399, https://doi.org/10.1246/cl.160757.

[25] T.P. Vales, I.W.T. Badon, H.-J. Kim, Multi-responsive hydrogels functionalized with a photochromic spiropyran-conjugated chitosan network, Macromol. Res. 26 (2018) 950–953, https://doi.org/10.1007/s13233-018-6126-9.

[26] K. Xiong, C. Yin, Y. Yue, F. Huo, A near-infrared ratiometric fluorescence probe base on spiropyran derivative for pH and its application in living cells, Spectrochim. Acta A 223 (2019), https://doi.org/10.1016/j.saa.2019.117350 117350.

[27] X. He, W. Xu, C. Xu, F. Ding, H. Chen, J. Shen, Reversible spiropyran-based chemosensor with pH-switches and application for bioimaging in living cells, Pseudomonas aeruginosa and zebrafish, Dyes Pigments 180 (2020), https://doi.org/10.1016/j.dyepig.2020.108497 108497.

[28] Z. Yang, F. Wang, H. Liu, Dual responsive spiropyran-ended poly(N-vinyl caprolactam) for reversible complexation with metal ions, J. Polym. Res. 26 (2019) 89–99, https://doi.org/10.1007/s10965-019-1747-z.

[29] F.B. Miguez, T.G. Menzonatto, J.F.Z. Netto, I.M.S. Silva, T. Verano-Braga, J.F. Lopes, F.B.D. Sousa, Photo-dynamic and fluorescent zinc complex based on spiropyran ligand, J. Mol. Struct. 1211 (2020), https://doi.org/10.1016/j.molstruc.2020.128105 128105.

[30] J. Kohl-Landgraf, M. Braun, C. Özçoban, D.P.N. Gonçalves, A. Heckel, J. Wachtveitl, Ultrafast dynamics of a spiropyran in water, J. Am. Chem. Soc. 134 (34) (2012) 14070–14077.

[31] L. Kong, H.L. Wong, A.Y.Y. Tam, W.H. Lam, L. Wu, V.W.W. Yam, Synthesis, characterization, and photophysical properties of bodipy-spirooxazine and -spiropyran conjugates: modulation of fluorescence resonance energy transfer behavior via acidochromic and photochromic switching, ACS Appl. Mater. Interfaces 6 (2014) 1550–1562, https://doi.org/10.1021/am404242a.
[32] L. Kortekaas, O. Ivashenko, J.T. van Herpt, W.R. Browne, A remarkable multitasking double spiropyran: bidirectional visible-light switching of polymer-coated surfaces with dual redox and proton gating, J. Am. Chem. Soc. 138 (2016) 1301–1312, https://doi.org/10.1021/jacs.5b11604.
[33] H. Zhang, F. Gao, X. Cao, Y. Li, Y. Xu, W. Weng, R. Boulatov, Mechanochromism and mechanical-force-triggered cross-linking from a single reactive moiety incorporated into polymer chains, Angew. Chem., Int. Ed. 128 (2016) 3092–3096, https://doi.org/10.1002/ange.201510171.
[34] P.K. Kundu, D. Samanta, R. Leizrowice, B. Margulis, H. Zhao, M. Börner, T. Udayabhaskararao, D. Manna, R. Klajn, Light-controlled self-assembly of non-photoresponsive nanoparticles, Nat. Chem. 7 (8) (2015) 646–652.
[35] K. Tomizaki, H. Mihara, Phosphate-mediated molecular memory driven by two different protein kinases as information input elements, J. Am. Chem. Soc. 129 (2007) 8345–8352, https://doi.org/10.1021/ja0703067.
[36] Y. Li, Y. Duan, J. Li, J. Zheng, H. Yu, R. Yang, Simultaneous nucleophilic-substituted and electrostatic interactions for thermal switching of spiropyran: a new approach for rapid and selective colorimetric detection of thiol-containing amino acids, Anal. Chem. 84 (2012) 4732–4738, https://doi.org/10.1021/ac203494e.
[37] F. Neese, The ORCA program system, Wiley Interdiscip. Rev. Comput. Mol. Sci. 2 (2012) 73–78, https://doi.org/10.1002/wcms.81.
[38] F. Neese, Software update: the ORCA program system, version 4.0, Wiley Interdiscip, Rev. Comput. Mol. Sci. 8 (2017) 73–78, https://doi.org/10.1002/wcms.1327.
[39] H. Kruse, S. Grimme, A geometrical correction for the inter- and intra-molecular basis set superposition error in Hartree-Fock and density functional theory calculations for large systems, J. Chem. Phys. 136 (2012), https://doi.org/10.1063/1.3700154.
[40] E. Caldeweyher, C. Bannwarth, S. Grimme, Extension of the D3 dispersion coefficient model, J. Chem. Phys. 147 (3) (2017) 034112.
[41] S. Grimme, A. Hansen, S. Ehlert, J.-M. Mewes, r2SCAN-3c: A "Swiss army knife" composite electronic-structure method, J. Chem. Phys. 154 (6) (2021) 064103.
[42] J.W. Furness, A.D. Kaplan, J. Ning, J.P. Perdew, J. Sun, Accurate and numerically efficient r2SCAN meta-generalized gradient approximation, J. Phys. Chem. Lett. 11 (2020) 8208–8215, https://doi.org/10.1021/acs.jpclett.0c02405.
[43] Y. He, B. Zhu, Y. Inoue, Hydrogen bonds in polymer blends, Prog. Polym. Sci. 29 (10) (2004) 1021–1051.
[44] R. Zhang, L. Hu, Z. Xu, Y. Song, H. Li, X. Zhang, X. Gao, M. Wang, C. Xian, A highly selective probe for fluorescence turn-on detection of Fe^{3+} ion based on a novel spiropyran derivative, J. Mol. Struct. 1204 (2020), 127481, https://doi.org/10.1016/j.molstruc.2019.127481.